

**Exchange interactions in (ZnMn)Se: LDA and LDA+U calculations**

L. M. Sandratskii\*

*Max-Planck Institut für Mikrostrukturphysik, D-06120 Halle, Germany*

(Received 11 March 2003; revised manuscript received 30 June 2003; published 29 December 2003)

One of the remarkable properties of the II-VI diluted magnetic semiconductor (ZnMn)Se is the giant spin splitting of the valence-band states under application of the magnetic field (giant Zeeman splitting). This splitting reveals strong exchange interaction between Mn moments and semiconductor states. On the other hand, no magnetic phase transition has been observed for systems with small Mn content up to very low temperatures. The latter property shows weakness of the exchange interaction between Mn moments. In this paper, the local-density approximation (LDA) and the LDA+U techniques are employed to study exchange interactions in (ZnMn)Se. Supercell and frozen-magnon approaches applied earlier to III-V diluted magnetic semiconductors are used. It is found that both LDA and LDA+U describe successfully the combination of the strong Zeeman splitting and weak-interatomic exchange. However, the physical pictures provided by two techniques differ strongly. A detailed analysis shows that the LDA+U method provides the description of the system which is much closer to the experimental data.

DOI: 10.1103/PhysRevB.68.224432

PACS number(s): 75.50.Pp, 75.30.Et, 71.15.Mb

**I. INTRODUCTION**

The perspective of using the spin of electrons in the semiconductor devices promises to revolutionize modern electronics.<sup>1</sup> A necessary component of a spintronic process is the spin injection into semiconductor. This demand creates a need for ferromagnetic materials on the semiconductor basis with strong spin polarization of the carriers and high Curie temperature. After recent discovery<sup>2</sup> of ferromagnetism in (GaMn)As with Curie temperature as high as 110 K much attention is devoted to the study of the diluted III-V semiconductors as possible sources of the spin-polarized electrons. Also the interest to more traditional II-VI semiconductors has been revived since, first, the theoretical studies show that the II-VI systems possess the potential for high Curie temperature;<sup>3,4</sup> second, the study of the II-VI diluted magnetic semiconductors (DMS) deepens understanding of the exchange interactions in other types of DMS (Refs. 4–6); and, third, the II-VI systems, in particular (ZnMn)Se, are used in spin-injection experiments as a source of spin-polarized charge carriers.<sup>7–9</sup>

In (ZnMn)Se with low Mn concentration no magnetic ordering has been experimentally detected down to very low temperatures.<sup>10</sup> However, the application of a magnetic field leads to the observation of the so-called giant Zeeman splitting for the states of the semiconductor matrix. Because of this large spin splitting (ZnMn)Se is an efficient source of highly polarized carriers.<sup>7,8</sup>

A commonly accepted explanation of the giant Zeeman splitting in (ZnMn)Se relies on the following picture. In the system there is a strong exchange interaction between the Mn 3*d* states and the states of the semiconductor. This interaction does not, however, lead to the ordering of the Mn moments. The application of a magnetic field aligns the Mn moments and results in the observation of a giant spin splitting. The term “giant” arises here from the comparison of two energy scales. The characteristic energy of the magnetostatic interaction of the magnetic field of 1 T with the spin of  $1\mu_B$  amounts to 0.004 mRy and is up to five orders of mag-

nitude smaller than the splittings detected experimentally.<sup>7,10</sup> The coexistence of a very strong exchange between the Mn 3*d* and semiconductor states and a very low temperature of the magnetic phase transition makes the II-VI DMS an interesting laboratory for studying the physics of exchange interactions.

Much effort has been paid to the theoretical studies of the DMS of the II-VI type (see, e.g., Refs. 4–6,10). Most of these studies are based on a model-Hamiltonian approach. (See, e.g., Ref. 11 for the model of bound magnetic polarons and Refs. 6 and 12 for the Zener model. The latter can be considered as a continuous-medium limit of the well-known Rudermann-Kittel-Kasuya-Yosida approach. Spalek *et al.*<sup>13</sup> used Anderson’s approach to superexchange and showed that few adjustable parameters of the theory are sufficient to describe the interplay between different types of exchange interactions in the system. A reach experimental information [e.g., Ref. 14 in the case of (ZnMn)Se] is helpful in the selection of the values of the parameters.)

The developments in the methods of the density-functional theory (DFT) accompanied by fast increasing computer power allow now for parameter-free calculation of the electronic properties of very complex systems. In the case of II-VI DMS the number of the DFT studies of the exchange interactions are still very restricted (for exceptions see, e.g., Refs. 4,15 and 16). Most of the calculations have been performed with the use of a virtual crystal approximation or a single-site coherent-potential approximation (CPA).<sup>4,15</sup> These schemes are convenient and efficient in the investigation of the systems with varying concentration of impurities. They, however, do not take into account the atomic short-range order and the increasing distance between impurities with decreasing impurity concentration. Therefore it is important to combine the calculations within the virtual-crystal and CPA techniques with the studies taking more detailed account of the positions of the impurity atoms. Such studies can be performed with the use of large supercells of the semiconductor crystals.<sup>17–20</sup> The aim of this paper is the investigation of the exchange interactions in (ZnMn)Se on

the basis of the supercell approach.

An important question concerns the role of the intra-atomic correlations in the Mn  $3d$  states. Within the model-Hamiltonian approaches the  $3d$  states are usually considered as atomlike and strongly correlated. This treatment is rather different from the treatment within local-density approximation (LDA). To study the role of the electron correlations in the Mn  $3d$  shell we use the LDA+U method<sup>21</sup> designed to take into account the on-site Coulomb interaction  $U$ .

The purpose of this paper is twofold. On the one hand, by detailed DFT calculations of the electronic properties of (ZnMn)Se we aim to provide deeper insight into the physics of the system. On the other hand, by comparison with the experimental data with the calculational results we aim to draw the conclusion which of the two approaches LDA or LDA+U provides a better description of (ZnMn)Se. Both components of the purpose are of strong importance for future studies of DMS within the DFT.

## II. CALCULATIONAL APPROACH

In the calculations we follow the scheme described in Ref. 18. This scheme is based on the supercell approach where one of the Zn atoms in a supercell of zinc-blende ZnSe is replaced by a Mn atom. The calculations are performed for four values of the concentration  $x$ : 0.25, 0.125, 0.0625, and 0.03125.

The calculations were carried out with the augmented spherical waves<sup>22</sup> (ASW) method within the LDA and LDA+U approaches. In all calculations the lattice parameter was chosen to be equal to the experimental lattice parameter of ZnSe. Two empty spheres per formula unit have been used in the calculations. The positions of empty spheres are (0.5, 0.5, 0.5) and (0.75, 0.75, 0.75). Radii of all atomic spheres were chosen to be equal. Depending on the concentration of Mn, the supercell is cubic ( $x=25\%$ ,  $a \times a \times a$ , and  $x=3.125\%$ ,  $2a \times 2a \times 2a$ ) or tetragonal ( $x=12.5\%$ ,  $a \times a \times 2a$  and  $6.25\%$ ,  $2a \times 2a \times a$ ).

The LDA+U calculations were performed with  $U=0.3$  Ry.<sup>23</sup>

### A. Spin-projected densities of states

The spin splitting of the valence-band states is a result of the interaction between these states and the Mn  $3d$  states. The directions of the Mn moments are disordered in the absence of a magnetic field and become increasingly ordered with increasing value of the applied field. There are two possible scenarios for the relation between the ordering of the Mn moments and the spin splitting of the valence-band states (Fig. 1). The first scenario is a mean-field (Stoner-like) type relation. In this case the valence-band states experience an average exchange field of the Mn moments that is proportional to the net magnetization in the Mn subsystem. Complete disordering of the Mn moments leads to the disappearance of the net magnetization and, as a consequence, of the spin splitting. In the second scenario, the spin of the valence states follows locally the spins of the Mn atoms. Therefore, the spin polarization and exchange splitting do not disappear

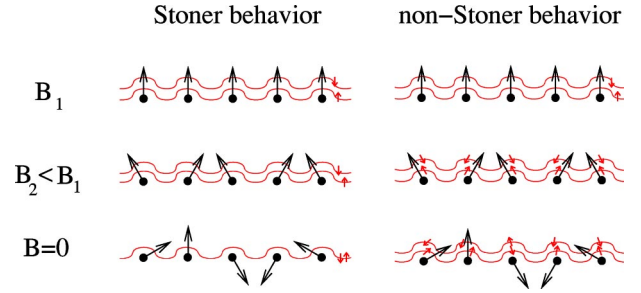


FIG. 1. (Color online) Two scenarios of the relation between the net magnetization due to the localized moments and the exchange splitting of the valence state. In the mean-field (Stoner-like) scenario the splitting is proportional to the net magnetization. The distance between wave lines shows schematically the value of the exchange splitting. In the non-mean-field (non-Stoner) scenario the spin of the valence electrons follows locally the direction of the Mn moments. In this case the exchange splitting is present also in the case of zero net magnetization.

with disappearance of the net magnetization. An experimental example of the non-Stoner behavior of the exchange splitting is discussed by Kisker<sup>24</sup> for the case of iron with thermally disordered atomic moments. In (ZnMn)Se the experimental data are treated in favor of the mean-field scenario.<sup>10</sup>

To study both scenarios within the DFT we will need to calculate densities of states (DOS) projected on different spin-quantization axes. The calculation is performed as follows. The wave function of a given electron state is considered to be a two-component spinor  $\begin{pmatrix} \psi_1(\mathbf{r}) \\ \psi_2(\mathbf{r}) \end{pmatrix}$ . The spin components  $\psi_1(\mathbf{r})$  and  $\psi_2(\mathbf{r})$  are written with respect to a chosen axis. The spin-quantization axis does not change within atomic spheres but can vary from atom to atom. The integral

$$n_{i\mathbf{k}\nu}^s = \int_{\Omega_\nu} d\mathbf{r} |\psi_{i\mathbf{k}\nu}(\mathbf{r})|^2 \quad (1)$$

gives the part of the state  $\psi_{i\mathbf{k}}$  corresponding to atom  $\nu$  and spin projection  $s$ . Here  $\mathbf{k}$  is the wave vector and  $i$  numbers the energy bands. The integration is carried out over the  $\nu$ th atomic sphere. The wave functions are normalized in the unit cell:  $\sum_{s\nu} n_{i\mathbf{k}\nu}^s = 1$ . The partial DOS for given  $\nu$  and  $s$  is given by the formula

$$N_\nu^s(\varepsilon) = \frac{1}{\Omega_{BZ}} \sum_i \int_{BZ} d\mathbf{k} n_{i\mathbf{k}\nu}^s \delta(\varepsilon - \varepsilon_{i\mathbf{k}}), \quad (2)$$

where  $\Omega_{BZ}$  is the volume of the Brillouin zone (BZ). To calculate the partial DOS with respect to another quantization axis the electron wave functions are subjected to the transformation<sup>25</sup>

$$\begin{pmatrix} \psi'_1(\mathbf{r}) \\ \psi'_2(\mathbf{r}) \end{pmatrix} = U_\nu^\dagger \begin{pmatrix} \psi_1(\mathbf{r}) \\ \psi_2(\mathbf{r}) \end{pmatrix}, \quad \mathbf{r} \in \Omega_\nu, \quad (3)$$

where  $U_\nu$  is the spin- $\frac{1}{2}$  transformation matrix corresponding to the rotation of the axis of the  $\nu$ th atom. Subsequently the

procedure defined by Eqs. (1) and (2) is performed for the spinor components of the transformed functions (3).

### B. Interatomic exchange parameters and Curie temperature

To describe the exchange interactions between Mn moments we use an effective Heisenberg Hamiltonian of classical spins

$$H_{eff} = - \sum_{i \neq j} J_{ij} \mathbf{e}_i \cdot \mathbf{e}_j, \quad (4)$$

where  $J_{ij}$  is an exchange interaction between two Mn sites ( $i, j$ ) and  $\mathbf{e}_i$  is the unit vector pointing in the direction of the magnetic moment at site  $i$ .

To estimate the parameters of the Mn-Mn exchange interaction we perform calculation for the following frozen-magnon<sup>26,27</sup> configurations:

$$\theta_i = \text{const}, \quad \phi_i = \mathbf{q} \cdot \mathbf{R}_i, \quad (5)$$

where  $\theta_i$  and  $\phi_i$  are the polar and azimuthal angles of vector  $\mathbf{e}_i$ , and  $\mathbf{R}_i$  is the position of the  $i$ th Mn atom. The directions of the induced moments in the atomic spheres of Zn and Se and in the empty spheres were kept to be parallel to the  $z$  axis.

It can be shown that within the Heisenberg model (4) the energy of such configurations can be represented in the form

$$E(\theta, \mathbf{q}) = E_0(\theta) - \theta^2 J(\mathbf{q}), \quad (6)$$

where  $E_0$  does not depend on  $\mathbf{q}$  and  $J(\mathbf{q})$  is the Fourier transform of the parameters of the exchange interaction between pairs of Mn atoms:

$$J(\mathbf{q}) = \sum_{j \neq 0} J_{0j} \exp(i\mathbf{q} \cdot \mathbf{R}_{0j}). \quad (7)$$

In Eq. (6) angle  $\theta$  is assumed to be small. Using  $J(\mathbf{q})$  one can estimate the energies of the spin-wave excitations:<sup>28</sup>

$$\omega(\mathbf{q}) = \frac{4}{M} [J(\mathbf{0}) - J(\mathbf{q})] = \frac{4}{M} \frac{E(\theta, \mathbf{q}) - E(\theta, \mathbf{0})}{\theta^2}, \quad (8)$$

where  $M$  is the atomic moment of the Mn atom. Performing back Fourier transformation we obtain the parameters of the exchange interaction between Mn atoms:

$$J_{0j} = \frac{1}{N} \sum_{\mathbf{q}} \exp(-i\mathbf{q} \cdot \mathbf{R}_{0j}) J(\mathbf{q}). \quad (9)$$

The Curie temperature was estimated in the mean-field (MF) approximation

$$k_B T_C^{MF} = \frac{2}{3} \sum_{j \neq 0} J_{0j}. \quad (10)$$

We use a rigid band approach to calculate the exchange parameters and Curie temperature for different electron occupations. We assume that the electron structure calculated for a DMS with a given concentration of the  $3d$  impurity is basically preserved in the presence of defects. The main dif-

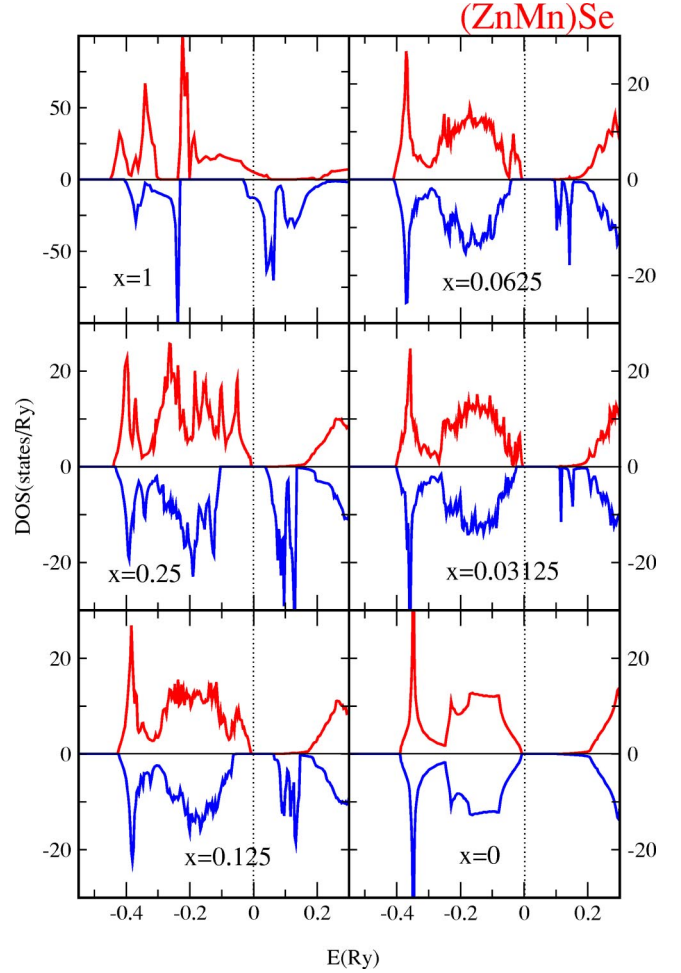


FIG. 2. (Color online) The DOS of  $\text{Zn}_{1-x}\text{Mn}_x\text{Se}$ . The DOS is given per unit cell of the zinc-blende crystal structure. The DOS above (below) the abscissas axis corresponds to the spin-up (-down) states.

ference is in the occupation of the bands and, therefore, in the position of the Fermi level.

## III. CALCULATIONAL RESULTS

### A. Densities of states and exchange splittings

#### 1. LDA

We begin the discussion of the calculational results with the consideration of the DOS of the ferromagnetic (ZnMn)Se (Fig. 2). Compared with pure ZnSe, the replacement of a Zn atom by a Mn atom adds five  $3d$  spin-up energy bands to the valence band of the system. Since the number of Mn  $3d$  electrons is also five no carriers appear either in the valence band or in the conduction band.

The values of the calculated spin moments are collected in Table I. The moment in the Mn sphere and the induced moment on the neighboring Se atom are practically independent of the Mn concentration. The moment per supercell is exactly  $5\mu_B$  since there are extra five filled spin-up bands compared with the nonmagnetic ZnSe.

TABLE I. Magnetic moments in  $\text{Zn}_{1-x}\text{Mn}_x\text{Se}$ . Shown are the Mn moment, the induced moment on the nearest Se atoms, and the magnetic moment of the supercell. All moments are in units of  $\mu_B$ .

	$x$			
	0.25	0.125	0.0625	0.03125
	LDA			
Mn	4.39	4.39	4.39	4.40
As	0.07	0.06	0.06	0.06
cell	5.0	5.00	5.00	5.00
	LDA+U			
Mn	4.52	4.51	4.51	4.51
As	0.06	0.05	0.05	0.05
cell	5.0	5.00	5.00	5.00

At the top of the valence band there is strong negative exchange splitting: the upper edge of the spin-up DOS lies higher in energy than the upper edge of the spin-down DOS (Fig. 2). The spin splitting increases with increasing Mn concentration. The origin of this splitting can be understood from the analysis of the partial Mn 3d DOS (Fig. 3). Indeed, a higher energy of the spin-up valence-band edge results

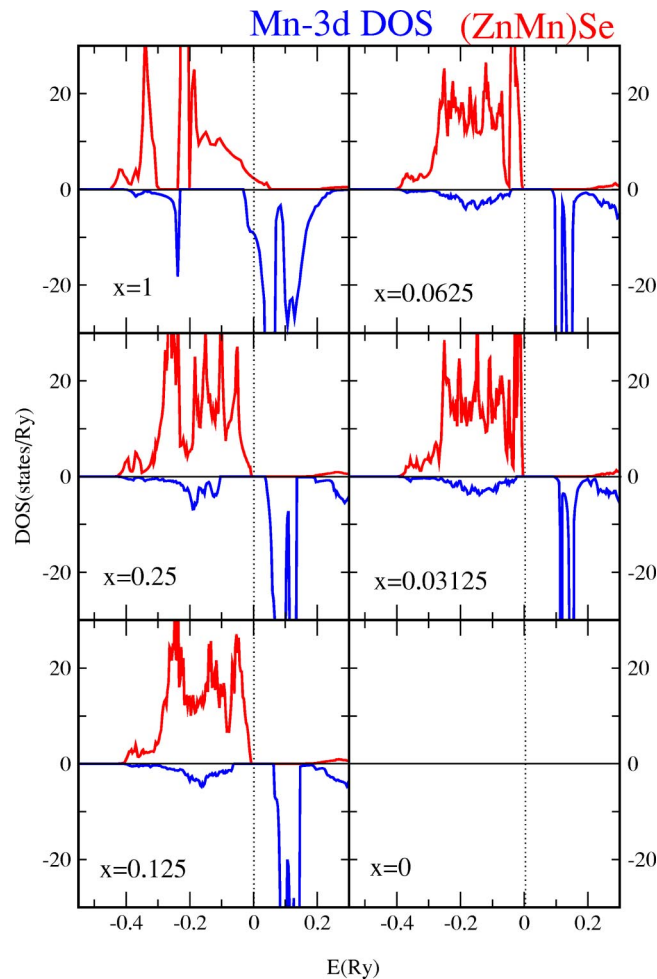


FIG. 3. (Color online) The partial Mn 3d DOS for  $\text{Zn}_{1-x}\text{Mn}_x\text{Se}$ . The DOS is given per Mn atom.

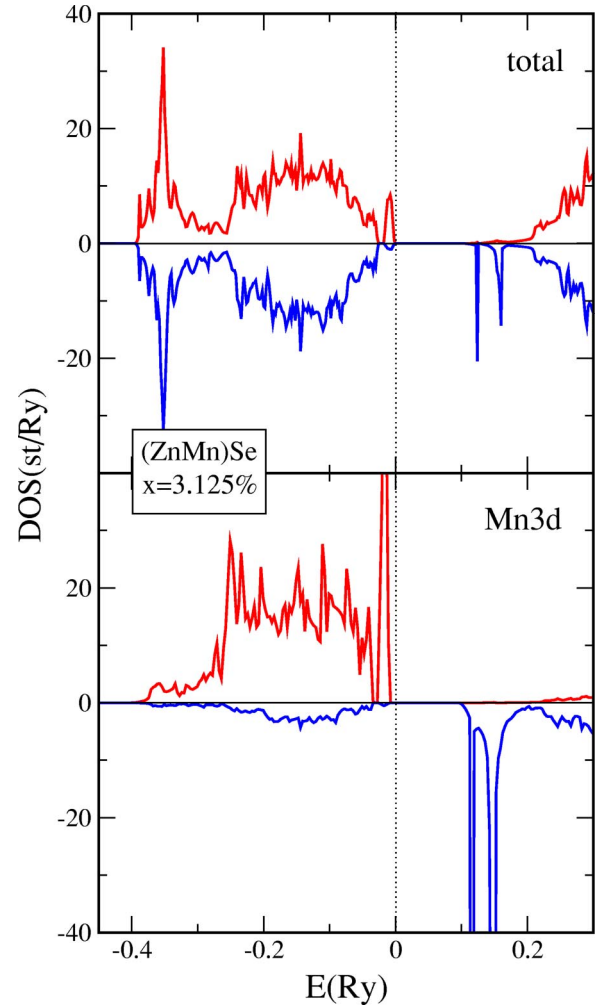


FIG. 4. (Color online) Total DOS and partial Mn 3d DOS for antiferromagnetic  $\text{Zn}_{1-x}\text{Mn}_x\text{Se}$  with  $x=3.125\%$ . The spin-projected DOS are calculated with respect to the local atomic quantization axes.

from the contribution of the Mn 3d spin-up states. On the other hand, there is no strong contribution of the Mn spin-down states to the valence band. Unoccupied spin-down Mn 3d bands lie in the semiconducting gap, close to the bottom of the conduction band.

The exchange splitting of the states at the top of the valence band of the ferromagnetic (ZnMn)Se is in qualitative agreement with the observation of the giant spin splitting under the application of the magnetic field.

To understand the dependence of the electron structure on the magnetic configuration we performed calculation for the antiferromagnetic configuration of the Mn moments for  $x=3.125\%$ . The antiferromagnetic structure is characterized by the largest angle between the neighboring Mn moments and, therefore, is the state most different from the ferromagnetic one. The comparison of the DOS of the ferromagnetic and antiferromagnetic configurations for  $x=3.125\%$  (Figs. 2 and 4) shows that they are similar. The main difference in the antiferromagnetic DOS is the appearance of a small energy gap which separates the upper part of the valence-band states from the rest of the valence band. The spin splitting obtained

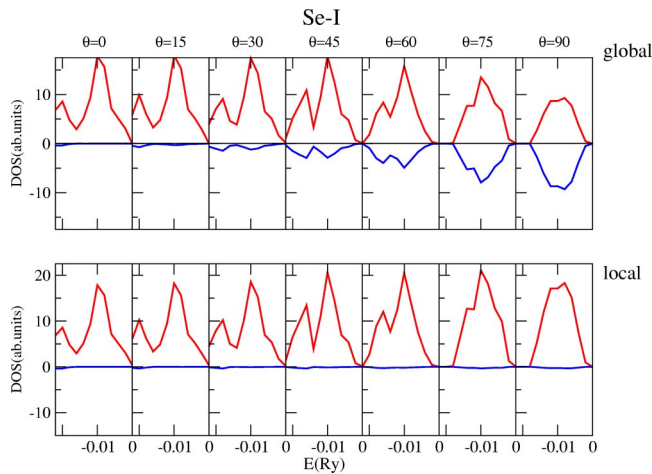


FIG. 5. (Color online) Fragment of the partial DOS of the Se-I atom at the top of the valence band for  $\text{Zn}_{0.96875}\text{Mn}_{0.03125}\text{Se}$ . Calculations are performed for seven magnetic configurations with different net magnetization. The upper part shows the spin projection on the global  $z$  axis. The lower part gives the spin projections on the axis parallel to the direction of the magnetic moment of the nearest Mn atom. No correlation between the spin splitting and the net magnetization can be established.

in the ferromagnetic DOS is present also in the antiferromagnetic DOS as the splitting between the top of the separated (impurity) band and the top of the valence band. Figures 3 and 4 show that the partial DOS of the Mn atoms are only weakly dependent on the magnetic configuration and preserve fully the local spin splitting. Obviously the main features of the LDA-DOS cannot be treated in terms of the Stoner-like mean-field picture (Fig. 1).

To study in more details the relation between the electron structure and magnetic configuration we next analyze the partial DOS of the atoms of the semiconductor matrix. As we will show below, the behavior of the DOS of different atoms

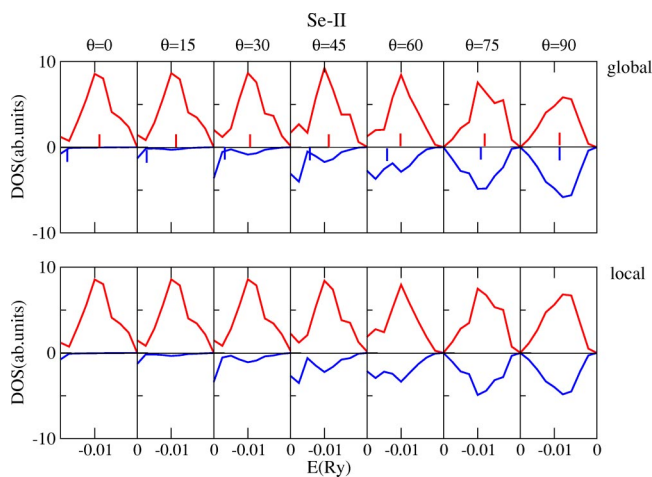


FIG. 6. (Color online) Fragment of the partial DOS of the Se-II atom. See the caption of Fig. 5 for details. Short vertical lines in the upper panel show the center of gravity for the corresponding spin projection. The decrease of the spin splitting with decreasing net magnetization can be established.

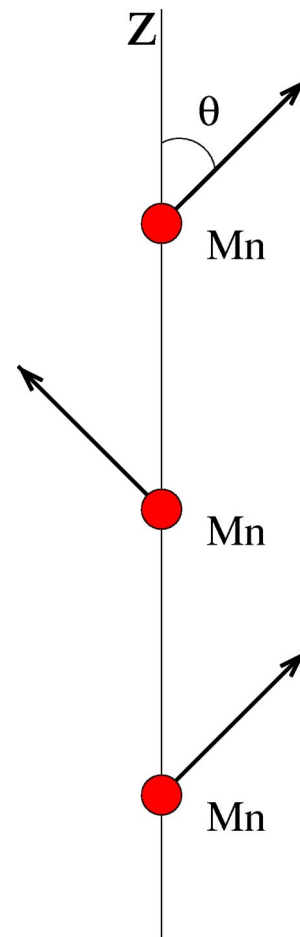


FIG. 7. (Color online) Schematic picture of the calculated magnetic configurations. Angle  $\theta$  assumed the following values:  $0^\circ$ ,  $15^\circ$ ,  $30^\circ$ ,  $45^\circ$ ,  $60^\circ$ ,  $75^\circ$ ,  $90^\circ$ . Calculations were performed for (ZnMn)Se with the Mn concentration of  $x = 3.125\%$ .

ranges from a highly non-Stoner one to the behavior well described by the mean-field picture.

In Figs. 5 and 6 we present the partial DOS for two different Se atoms. The DOS is calculated for magnetic configurations depicted schematically in Fig. 7 where three successive Mn atoms along the  $z$  axis are shown. The angles between neighboring Mn moments varies from  $0$  to  $180^\circ$  with a step of  $30^\circ$ . Correspondingly, the net magnetization varies from maximal to zero.

First of the two Se atoms, Se-I, is at position  $(a/4, a/4, a/4)$  and is the nearest neighbor of the Mn impurity situated at  $(0, 0, 0)$ . The second atom, Se-II, is at position  $(3a/4, 3a/4, 5a/4)$  and belongs to the fourth coordination sphere of Se atoms. (To remind the reader, the supercell in this case is a cube of the size  $2a$ .) The spin-projected DOS is presented with respect to two different quantization axes. The first (local) axis is parallel to the direction of the magnetic moment of the nearest Mn atom. The second (global) axis is directed along the net magnetization. The DOS projected on the local atomic quantization axis provides, in most cases, better insight into the physics of the system. However, in the experiments determining the spin splittings the spin-quantization axis is usually the global one.

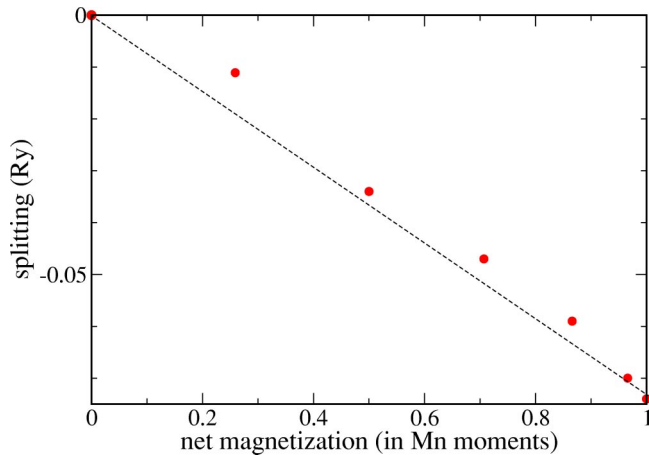


FIG. 8. (Color online) The exchange splitting calculated from the partial DOS of the Se-II atom as a function of the net magnetization. Negative value of the splitting reflects higher-energy position of the spin-up states. The dashed straight line is a guide for the eye.

The DOS shown in Figs. 5 and 6 reveal strong difference between two Se atoms. The spin of the electron states of the Se-I atom follows almost perfectly the spin of the neighboring Mn atom (Fig. 5). This is evidenced by the negligibly small local spin-down DOS. The smallness of the local spin-down DOS holds up to the largest angle between Mn moments. Considered from the viewpoint of the global quantization axis, both spin-up and spin-down DOS of Se-I have similar shape but different weights (amplitudes). The relative weight of the spin-down DOS increases from zero for  $\theta = 0^\circ$  to 1 for  $\theta = 90^\circ$ . Because of the similarity of the form of the global spin-up and spin-down DOS the variation of the DOS with the change of the net magnetization cannot be treated in terms of the varied spin splitting. The changes in the global DOS take the form of the redistribution of the weight between the spin-up and spin-down DOS. This behavior is principally different from the behavior expected within the mean-field picture.

On the other hand, for Se-II we get a strong dependence of the local DOS on the magnetic configuration of the Mn moments (Fig. 6). With increasing angle between Mn moments the contribution of the spin-down DOS increases. This happens because the spin of the states of Se-II deviates increasingly from the spin of the nearest Mn atom responding to the influence of other Mn atoms. Now, the shapes of the spin-up and spin-down DOS calculated with respect to the global quantization axis differ strongly. To characterize this difference in terms of the spin splitting we calculated the centers of gravity for both spin DOS in the energy region at the top of the valence band (Fig. 6). In a good approximation the spin splitting is proportional to the net magnetization (Fig. 8). Therefore the properties of the electron structure of Se-II can be described within the mean-field picture.

Since the relation between the exchange splitting and net magnetization varies from atom to atom, in experiments probing different parts of the electron structure this relation can appear different.

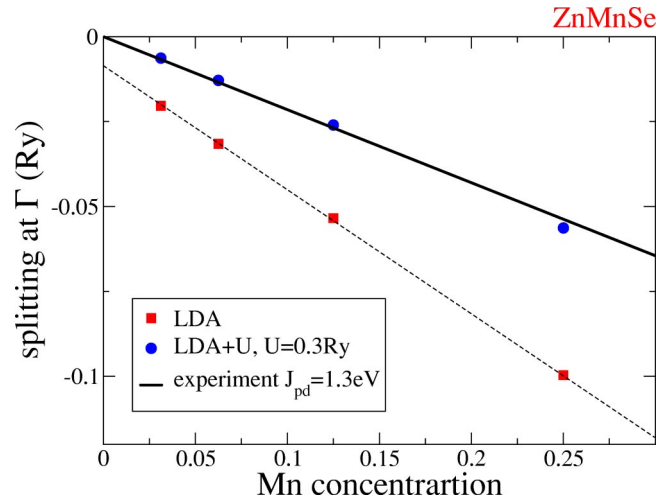


FIG. 9. (Color online) The exchange splitting at the top of the valence band ( $\Gamma$  point). Calculations are performed within LDA and LDA+U. The solid line corresponds to the experimental value of the  $J_{pd}$  parameter (Ref. 5).

An important role in the experimental determination of the strength of the exchange interaction between the Mn moments and valence-band states in DMS is played by the magneto-optical measurements of the spin splitting at the top of the valence band ( $\Gamma$  point of the Brillouin zone).<sup>10</sup> In Fig. 9 we show the calculated dependence of the splitting on Mn concentration. The LDA results for the exchange splitting at the  $\Gamma$  point disagree with experiment in two respects. First, the mean-field picture which assumes proportionality between the exchange splitting and the net magnetization in the system does not apply to the LDA results. The LDA splitting is well described by a linear function with a finite value in the limit of  $x \rightarrow 0$ . Such form of the dependence is the result of the presence of the Mn 3d states at the Fermi level. Second, the exchange splitting is substantially larger than the splitting obtained experimentally. Since the LDA results cannot be described within the mean-field picture the use of the formula

$$J_{pd} = \frac{\Delta E}{Sx} \quad (11)$$

gives values of the  $J_{pd}$  parameter that depend on concentration  $x$ . For illustration, the value of  $J_{pd}$  obtained for  $x = 0.125$  according to Eq. (11) is about two times larger than the experimental value. In Eq. (11),  $\Delta E$  is the exchange splitting and  $S$  is the atomic spin moment of Mn.

## 2. LDA+U

Introducing the Hubbard-U into the calculational scheme results in a strong shift of the Mn 3d spin-up states to lower energies (Figs. 10 and 11). At the top of the valence band there is still an admixture of the Mn 3d states. It is, however, very weak, especially for the spin-up states. Nevertheless, one can notice the hybridizational repulsion of the valence-band spin-down states from the spin-down Mn 3d states lying in the semiconductor gap. This repulsion is an important

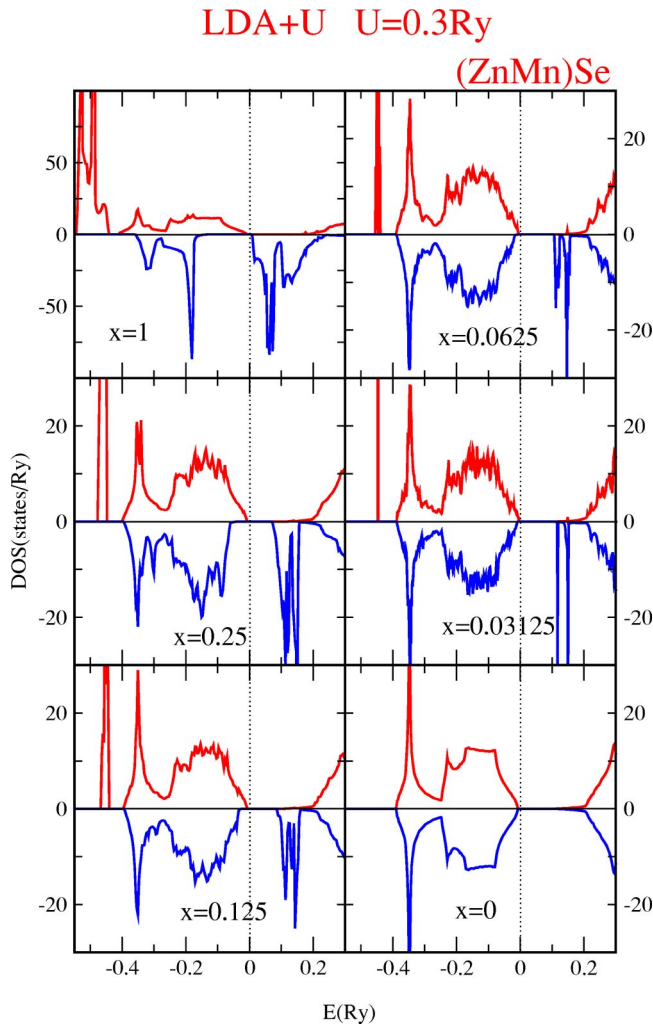


FIG. 10. (Color online) The DOS of  $\text{Zn}_{1-x}\text{Mn}_x\text{Se}$  calculated within the LDA+U approach with  $U=0.3$  Ry. (To compare with Fig. 2 presenting LDA calculation.)

factor leading, in agreement with experiment, to negative exchange splitting at the top of the valence band. Note that in the LDA calculation the negative exchange splitting has a different origin: the presence of the spin-up Mn  $3d$  states at the top of the valence band.

To study the relation between net magnetization and exchange splitting we performed calculation for the antiferromagnetic configuration of the Mn moments for  $x=3.125\%$  (Fig. 12). In contrast to LDA (Fig. 4), no exchange splitting of the states at the top of the valence band is obtained in the antiferromagnetic case. This property is in agreement with the mean-field picture (Fig. 1). To investigate this property further we performed the LDA+U calculation of the exchange splitting at the  $\Gamma$  point of the BZ as a function of the Mn concentration  $x$  (Fig. 9). The result obtained within the LDA+U scheme is in very good agreement with the experiment concerning both the mean-field character of the dependence and the magnitude of the exchange parameter  $J_{pd}$ . Summarizing the study of the exchange interaction between Mn  $3d$  and valence-band states we conclude that the LDA+U approach provides for this property much better

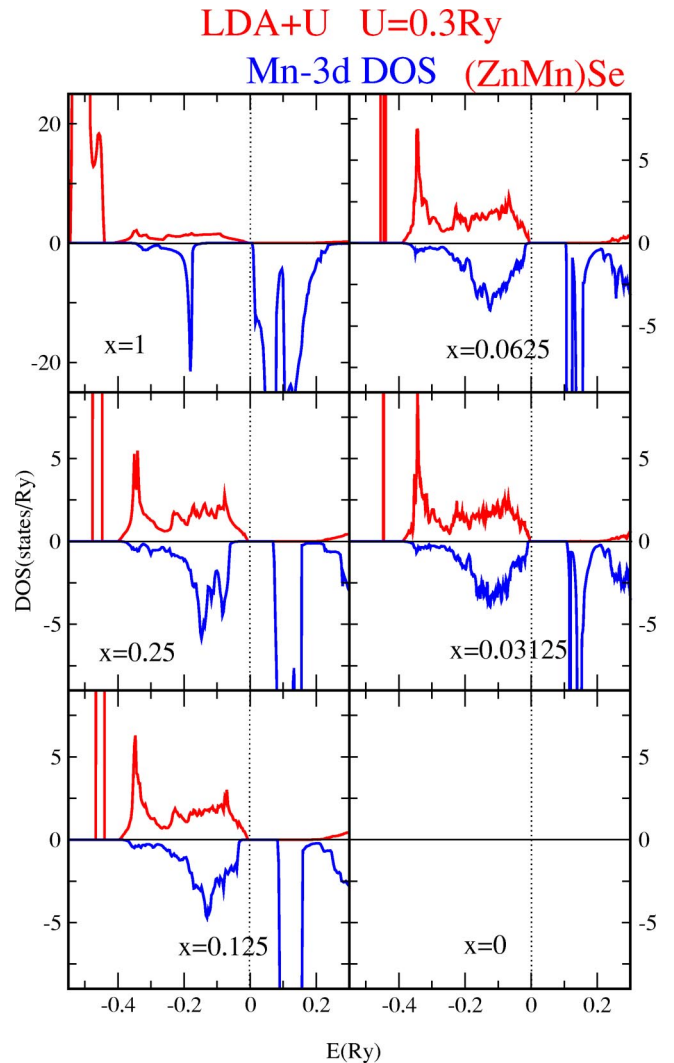


FIG. 11. (Color online) The partial Mn  $3d$  DOS for  $\text{Zn}_{1-x}\text{Mn}_x\text{Se}$  calculated within the LDA+U approach with  $U=0.3$  Ry. (To compare with Fig. 3 presenting LDA calculation. Notice the change in the scale of the ordinate axis that reflects strong change in the DOS.)

agreement with the experiment than the LDA approach.

## B. Interatomic exchange interactions

Now we turn to the discussion of the exchange interactions between Mn moments and address the question why large Mn moments and strong  $p$ - $d$  exchange do not result in the case of (ZnMn)Se with low Mn content in a sizable magnetic phase-transition temperature. To get deeper insight into the formation of the interatomic exchange interactions in the system we performed calculations for different band occupations (Fig. 13). The number of electrons varied from  $n=-2$  (two electrons per supercell less) to  $n=0$ . Negative values of the Curie temperature in Fig. 13 indicate an instability of the ferromagnetic state due to dominating antiferromagnetic interactions. The calculations have been performed within both LDA and LDA+U approaches. In Fig. 14 we

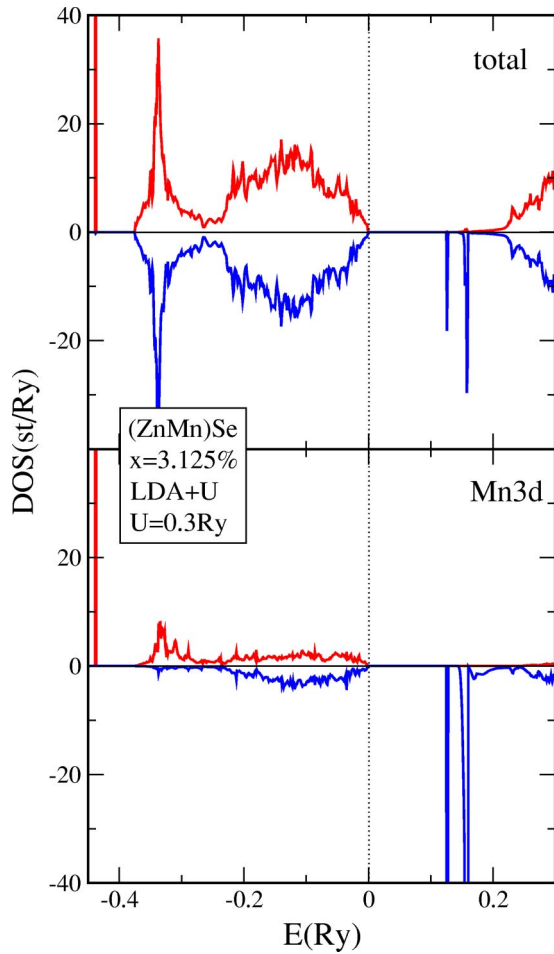


FIG. 12. (Color online) Total DOS and partial Mn  $3d$  DOS for the antiferromagnetic  $\text{Zn}_{1-x}\text{Mn}_x\text{Se}$  with  $x=3.125\%$  calculated within LDA+U approach. The spin-projected DOS are calculated with respect to the local atomic quantization axes.

show, for  $x=3.125\%$ , the dependence of the main interatomic exchange parameters as a function of the valence-band occupation.

We begin with the discussion of the features common for both LDA and LDA+U calculations. Analysis of the calculated  $T_C^{MF}$  (Fig. 13) shows that in the case of a completely filled valence band and empty conduction band ( $n=0$ ) the main exchange interactions are antiferromagnetic. The antiferromagnetic character of the interaction agrees with the commonly expected picture that the interatomic exchange interaction between magnetic atoms in an insulating system is dominated by the antiferromagnetic superexchange. This interaction is considered to be mediated by the states of the intermediate nonmagnetic atoms<sup>29</sup> or the states of the completely filled bands.<sup>15</sup>

Remarkable, however, is the very small value of the exchange interactions for  $n=0$ . With decreasing number of the holes the absolute value of all interatomic exchange interactions becomes very small. This result is in good correlation with the failure to experimentally detect the spin ordering up to very low temperatures.<sup>10</sup> It is also in agreement with the perturbative calculation by Larsen *et al.* for  $\text{Cd}_{1-x}\text{Mn}_x\text{Te}$ .<sup>15</sup>

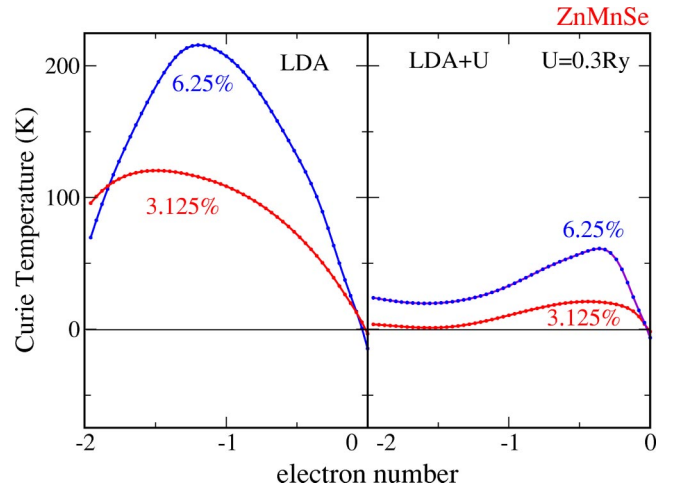


FIG. 13. (Color online)  $T_C^{MF}$  of (ZnMn)Se as a function of the electron number  $n$ .  $n=0$  corresponds to the nominal electron number in (ZnMn)Se. For  $n=0$  there is no charge carrier in the system.

The calculations show that the appearance of holes results in increasing ferromagnetic interactions. This is reflected by the property that the minimum of the estimated  $T_C$  is at  $n=0$  (Fig. 13) and correlates with experimental observation of the ferromagnetism with small Curie temperature in  $p$ -doped (ZnMn)Te.<sup>12</sup>

Although both LDA and LDA+U give very weak negative exchange interactions for a completely filled valence band the form of the dependence of the interatomic exchange parameters and correspondingly Curie temperature on the number of holes differs strongly for these two techniques (Figs. 13 and 14). Comparison of the calculated exchange parameters shows that the main difference between LDA and LDA+U concerns parameter  $J_{022}$  that describes the exchange interaction between the Mn atoms separated by vector (022): the LDA predicts a much stronger increase of the ferromagnetic interaction than LDA+U. The strength of the ferromagnetic interactions obtained within LDA seems to be

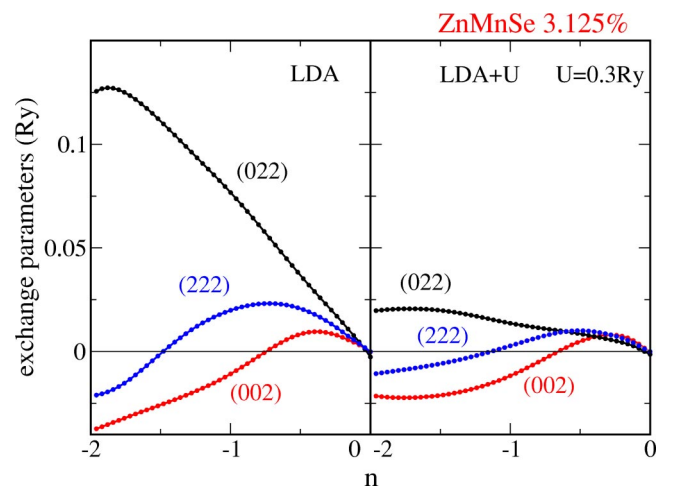


FIG. 14. (Color online) The main interatomic exchange parameters of (ZnMn)Se with Mn concentration of  $x=3.125\%$  as a function of the electron number.

strongly overestimated since the large values of the LDA  $T_C$  (Fig. 13) do not correlate with the experimental data available. On this basis, we conclude that the LDA+U scheme gives a better description of the character of the dependence of the interatomic exchange interactions on the number of holes.

This last conclusion might seem to be expected since in Sec. III A we have seen that the value of the  $J_{pd}$  parameter playing an important role in the mediation of the ferromagnetism is overestimated by LDA. The situation is, however, more complex since a larger  $J_{pd}$  parameter is accompanied, in the case of LDA, by a stronger spatial localization of the valence-band hole states about the Mn atom. Increased localization of the holes produces the trend to decreasing  $T_C$ . Which of the two factors,  $J_{pd}$  or hole localization, prevails depends on the peculiar interplay of the details of the electron structure of the specific system studied. The calculations for various III-V DMS show that the account for Hubbard-U can lead to both increase and decrease of the Curie temperature.<sup>30</sup>

To complete the consideration of the exchange interactions in (ZnMn)Se we discuss the physical reason for a very weak interatomic exchange interactions for undoped (ZnMn)Se ( $n=0$  in Fig. 13). To remind the reader, this result is common for both LDA and LDA+U and is very important for understanding of the failure to experimentally detect any magnetic phase transition down to very low temperatures. Note that the behavior of the II-VI DMS is different from

that obtained for the III-V DMS (GaMn)As. In (GaMn)As, the same calculational scheme gives<sup>19</sup> for the completely filled valence band and  $x=3.125\%$  interatomic antiferromagnetic interactions that are about 20 times larger than in (ZnMn)Se (Fig. 13).

To understand the weakness of the calculated superexchange in (ZnMn)Se and the difference between (ZnMn)Se and (GaMn)As we invoke a tight-binding model of noncollinear magnetic configurations. We consider helical configurations of the atomic moments and study the dependence of the band energy of the system on magnetic structure. The helical structures are defined by the formula

$$\mathbf{e}_n = [\cos(\mathbf{q} \cdot \mathbf{R}_n) \sin \theta, \sin(\mathbf{q} \cdot \mathbf{R}_n) \sin \theta, \cos \theta], \quad (12)$$

where  $\mathbf{R}_n$  are the lattice vectors,  $\mathbf{q}$  is the wave vector of the helix,  $\mathbf{e}_n$  is the unit vectors in the direction of the magnetic moment at site  $\mathbf{R}_n$ , and the polar angle  $\theta$  gives the deviation of the moments from the  $z$  axis. The helical structures allow to describe a broad range of magnetic configurations from collinear ferromagnetism ( $\theta=0$  or  $\mathbf{q}=\mathbf{0}$ ) to collinear antiferromagnetism ( $\mathbf{q}=\frac{1}{2}\mathbf{K}$  and  $\theta=90^\circ$ ,  $\mathbf{K}$  is a reciprocal lattice vector).

The tight-binding method for spiral structures was discussed in its general form in Ref. 31. By neglecting the difference in the spatial dependence of the basis functions with opposite spin projections and by preserving only the single-center matrix elements of the exchange potential we arrive at the following simple form of the secular matrix  $H(\mathbf{k})$ :<sup>32</sup>

$$H(\mathbf{k}) = \begin{pmatrix} \cos^2 \frac{\theta}{2} H_- + \sin^2 \frac{\theta}{2} H_+ - \frac{1}{2} \Delta & -\frac{1}{2} \sin \theta (H_- - H_+) \\ -\frac{1}{2} \sin \theta (H_- - H_+) & \sin^2 \frac{\theta}{2} H_- + \cos^2 \frac{\theta}{2} H_+ + \frac{1}{2} \Delta \end{pmatrix}, \quad (13)$$

where  $H_- = H_0(\mathbf{k} - \frac{1}{2}\mathbf{q})$ ,  $H_+ = H_0(\mathbf{k} + \frac{1}{2}\mathbf{q})$ , and matrix  $H_0(\mathbf{k})$  describes spin-degenerate bands of a nonmagnetic crystal;  $\Delta$  is the diagonal matrix of the on-site exchange splittings. In LDA+U scheme  $\Delta$  includes also  $U/2$ . Secular matrix (13) describes a many-band system and takes into account the hybridization between the states of different atoms. Through the hybridization between the Mn states and the states of the semiconductor matrix the spin polarization is transmitted to the nonmagnetic atoms. Note that in contrast to the two-band model used in Ref. 19 the matrix (13) includes all relevant bands. In particular the Mn  $3d$  states are assumed to be included. This makes model (13) conceptually similar to our ASW calculations.

The property of the secular matrix (13) that is important for us reads

$$\int_{\text{BZ}} d\mathbf{k} S p[H(\mathbf{k})] = 2 \int_{\text{BZ}} d\mathbf{k} H_0(\mathbf{k}), \quad (14)$$

that is, the trace of the matrix  $H(\mathbf{k})$  does not depend on the magnetic configuration. The variation of the magnetic structure changes the energy of individual electron states. The changes of different states, however, compensate. In the case when the trace of the secular matrix represents the total energy of the system the invariance with respect to the magnetic configuration means that all effective interatomic exchange interactions are negligible.

The property given by Eq. (14) applies to the total energy of a system if all bands described by the tight-binding secular matrix (13) are occupied. This condition can be fulfilled only in the case when the hybridization between the occupied and empty states is weak and can be neglected. The weakness of the hybridization allows us to include into the secular matrix the occupied states only.

An attempt to use Eq. (14) for the explanation of the weakness of the superexchange in (ZnMn)Se leads immediately to the following difficulty. According to Eq. (13) both spin-up and spin-down Mn  $3d$  states must be included into the secular matrix to fulfill Eq. (14). Since only the spin-up

Mn  $3d$  states are occupied, the inclusion of the spin-down Mn  $3d$  states, apparently, does not allow us to relate the trace of the matrix to the energy of the system. In the case of (ZnMn)Se this difficulty can, however, be overcome if we notice that the spin-down Mn  $3d$  states form very narrow energy bands lying in the semiconducting gap of ZnSe (Figs. 2 and 10). For example, the estimation for the LDA case shows that the states of these bands are strongly localized about the Mn atoms: more than 76% is located in the Mn spheres and more than 88% within the first coordination sphere of the Zn atoms. These states can be treated as evanescent states that are unable to mediate efficiently the exchange interaction between Mn atoms (Fig. 13). The evanescent character of the empty Mn  $3d$  states allows us to approximately consider their contribution into the trace of the secular matrix [Eq. (14)] as being independent of the magnetic configuration. This has as a consequence that the contribution of the occupied states is also approximately independent of the magnetic configuration resulting in weak effective interatomic exchange interactions.

This consideration allows us to also explain the difference between DMS on the GaAs and ZnSe bases. The semiconducting energy gap is substantially larger in the case of ZnSe. In the case of GaAs the influence of empty states is stronger and they must be included into the secular matrix (13). Therefore, the property described by Eq. (14) does not apply to the occupied states that results in stronger superexchange.

Some further comments are worth making here. First, the relation between the value of the semiconducting gap and the spatial extent of the exchange interactions has been discussed many times in the scientific literature within the framework of the perturbative treatment involving virtual transitions between the occupied states of the valence band and empty states of the conduction band. (See, e.g., Ref. 33 for an early publication on this topic. See also an interesting comment on the relation between the range of the exchange interaction and an imaginary Fermi vector in a recent paper by Pajda *et al.*<sup>34</sup>) The model considered above captures ba-

sically the same physics by taking into account, in a nonperturbative manner, the hybridization between occupied and empty states. Only in the case when the contribution of this hybridization to the response of the valence band states on the change of magnetic configuration is small the interatomic exchange interactions are weak. An important feature of model (13) is that it reflects the properties of the nonperturbative technique we used in the calculation of the exchange interactions and, therefore, provides additional understanding of the calculational results.

#### IV. CONCLUSIONS

One of the remarkable properties of the II-VI diluted magnetic semiconductor (ZnMn)Se is the giant spin splitting of the valence-band states under application of a magnetic field (giant Zeeman splitting). This splitting reveals strong exchange interaction between Mn moments and semiconductor states. On the other hand, no magnetic phase transition has been observed for systems with small Mn content down to very low temperatures. The latter property shows the weakness of the exchange interaction between Mn moments. In this paper, the LDA and the LDA+U techniques are employed to study exchange interactions in (ZnMn)Se. Supercell and frozen-magnon approaches applied earlier to III-V diluted magnetic semiconductors are used. It is found that both LDA and LDA+U describe successfully the combination of the strong Zeeman splitting and weak interatomic exchange. However, the physical pictures provided by two techniques differ strongly. A detailed analysis shows that LDA+U method provides a description of the system which is much closer to the experimental data.

#### ACKNOWLEDGMENTS

The author profited much from the discussions with Patrick Bruno and Tomasz Dietl. The financial support of Bundesministerium für Bildung und Forschung is acknowledged.

\*Electronic address: lsandr@mpi-halle.de

<sup>1</sup>H. Ohno, *Science* **281**, 951 (1998).

<sup>2</sup>H. Ohno, A. Shen, F. Matsukura, A. Oiwa, A. Endo, S. Kutsu-moto, and Y. Iye, *Appl. Phys. Lett.* **69**, 363 (1996).

<sup>3</sup>T. Dietl, H. Ohno, F. Matsukura, J. Cibert, and D. Ferrand, *Science* **287**, 1019 (2000)

<sup>4</sup>K. Sato and H. Katayama-Yosida, *Semicond. Sci. Technol.* **17**, 367 (2002).

<sup>5</sup>P. Kacman, *Semicond. Sci. Technol.* **16**, R25 (2001).

<sup>6</sup>T. Dietl, *Semicond. Sci. Technol.* **17**, 377 (2002).

<sup>7</sup>R. Fiederling, M. Keim, G. Reuscher, W. Ossau, G. Schmidt, A. Waag, and L.W. Molenkamp, *Nature (London)* **402**, 787 (1999); C. Gould, G. Schmidt, G. Richter, R. Fiederling, P. Grabs, and L.W. Molenkamp, *Appl. Surf. Sci.* **190**, 395 (2002).

<sup>8</sup>B.T. Jonker, Y.D. Park, B.R. Bennett, H.D. Cheong, G. Kioseoglou, and A. Petrou, *Phys. Rev. B* **62**, 8180 (2000).

<sup>9</sup>M. Oestreich, J. Hübner, D. Hägele, P.J. Klar, W. Heimbrodt, D.E. Ashenford, B. Lunn, and W.W. Rühle, *Appl. Phys. Lett.* **74**, 1251 (1999).

<sup>10</sup>J.K. Furdyna, *J. Appl. Phys.* **64**, R29 (1988).

<sup>11</sup>A.C. Durst, R.N. Bhatt, and P.A. Wolff, *Phys. Rev. B* **65**, 235205 (2002).

<sup>12</sup>D. Ferrand, J. Cibert, A. Wasiela, C. Bourgognon, S. Tatarenko, G. Fishman, T. Andrearczyk, J. Jaroszynski, S. Kolesnik, T. Dietl, B. Barbara, and D. Dufeu, *Phys. Rev. B* **63**, 085201 (2001)

<sup>13</sup>J. Spalek, A. Lewicki, Z. Tarnawski, J.K. Furdyna, R.R. Galazka, and Z. Obuszko, *Phys. Rev. B* **33**, 3407 (1986).

<sup>14</sup>J.K. Furdyna, N. Samarth, R.B. Frankel, and J. Spalek, *Phys. Rev. B* **37**, 3707 (1988).

<sup>15</sup>B.E. Larson, K.C. Hass, H. Ehrenreich, and A.E. Carlsson, *Phys. Rev. B* **37**, 4137 (1988).

<sup>16</sup>S.-H. Wei and A. Zunger, *Phys. Rev. B* **35**, 2340 (1987).

<sup>17</sup>S. Sanvito, G.J. Theurich, and N.A. Hill, *J. Supercond.* **15**, 85 (2002).

<sup>18</sup>L.M. Sandratskii and P. Bruno, *Phys. Rev. B* **66**, 134435 (2002).

<sup>19</sup>L.M. Sandratskii and P. Bruno, *Phys. Rev. B* **67**, 214402 (2003).

<sup>20</sup>Y.-J. Zhao, T. Shishidou, and A.J. Freeman, *Phys. Rev. Lett.* **90**,

- 047204 (2003); Y.-J. Zhao, W.T. Geng, K.T. Park, and A.J. Freeman, *Phys. Rev.* **64**, 35207 (2001).
- <sup>21</sup>V.I. Anisimov, I.V. Solovyev, M.A. Korotin, M.T. Czyzyk, and G.A. Sawatzky, *Phys. Rev. B* **48**, 16 929 (1993).
- <sup>22</sup>A.R. Williams, J. Kübler, and C.D. Gelatt, *Phys. Rev. B* **19**, 6094 (1979).
- <sup>23</sup>For the present calculation I selected the value of  $U \sim 4$  eV that is similar to the values used earlier [ J.H. Park, S.K. Kwon, and B.I. Min, *Physica B* **281282**, 703 (2000); J. Kudrnovsky (unpublished)] in the LDA+U calculations for III-V DMS; More efforts must be made in the future to determine U within a first-principles calculational scheme [see, e.g., V.I. Anisimov and O. Gunnarsson, *Phys. Rev. B* **43**, 7570 (1991)]. The present choice of  $U$  is additionally justified by good agreement with experiment. On the other hand, the comparison of the LDA calculation corresponding to  $U=0$  and LDA+U calculation for selected  $U$  allows easily to predict the trend in the variation of the calculated properties with variation of  $U$ .
- <sup>24</sup>E. Kisker, in *Metallic Magnetism*, edited by H. Capellmann (Springer-Verlag, Berlin, 1987), p. 57.
- <sup>25</sup>L.M. Sandratskii, *Adv. Phys.* **47**, 91 (1998).
- <sup>26</sup>S.V. Halilov, H. Eschrig, A.Y. Perlov, and P.M. Oppeneer, *Phys. Rev. B* **58**, 293 (1998).
- <sup>27</sup>Q. Niu and L. Kleinman, *Phys. Rev. Lett.* **80**, 2205 (1998).
- <sup>28</sup>Numerically it is advantageous to replace  $[E(\theta, \mathbf{q}) - E(\theta, \mathbf{0})]/\theta^2$  in Eq. (8) by  $[E(\theta, \mathbf{q}) - E(\theta, \mathbf{0})]/2(1 - \cos \theta)$  or  $[E(\theta, \mathbf{q}) - E(\theta, \mathbf{0})]/\sin^2 \theta$  that give proportionality between the numerator and the denominator of the ratio for larger interval of  $\theta$ .
- <sup>29</sup>P. W. Anderson, in *Magnetism I*, edited by Rado and Suhl (Academic Press, New York, 1963).
- <sup>30</sup>L. M. Sandratskii (unpublished).
- <sup>31</sup>L.M. Sandratskii, *Phys. Status Solidi B* **135**, 167 (1986).
- <sup>32</sup>L.M. Sandratskii and E.N. Kuvaldin, *J. Phys.: Condens. Matter* **3**, 7663 (1991).
- <sup>33</sup>N. Bloembergen and T.J. Rowland, *Phys. Rev. B* **97**, 1679 (1955).
- <sup>34</sup>M. Pajda, J. Kudrnovsky, I. Turek, V. Drchal, and P. Bruno, *Phys. Rev. B* **64**, 174402 (2001).